A *Caenorhabditis elegans* tissue model of radiation-induced reproductive cell death

J. B. Weidhaas*†, D. M. Eisenmann‡, J. M. Holub§, and S. V. Nallur*

*Department of Therapeutic Radiology, Yale University School of Medicine, New Haven, CT 06520; ‡Department of Biological Sciences, University of Maryland, Baltimore, MD 21201; and §Department of Biochemistry, New York University, New York, NY 10012

Communicated by P. Roy Vagelos, Merck & Co., Inc., Bedminster, NJ, May 10, 2006 (received for review March 28, 2006)

We have developed a tissue model of radiation-induced reproductive cell death in the nematode *Caenorhabditis elegans*. Reproductive cell death is the primary mode of death in tissue multipotential precursor cells, or ''clonogens,'' the targets of cytotoxic therapy, whose elimination results in normal tissue damage as well as solid-tumor eradication. Through extensive morphologic and genetic analysis, we have confirmed that cell death in this model represents reproductive cell death in isolation from apoptotic cell death, affording the opportunity to define the genetic pathways required for protection from reproductive cell death. We have additionally found that the DNA damage response pathway is necessary for protection from reproductive cell death, supporting the long-held tenet that DNA damage is the cause of reproductive cell death and further validating this model. This genetic tissue model provides a valuable tool for oncology-based research and affords a platform to broaden our insight into responses to cytotoxic therapy in tissues.

cytotoxic therapy | DNA damage response | genetic pathways | Radelegans

Radiation therapy is one of the three primary modalities used in the treatment of cancer. Although radiation has been in practice for over a century, the precise mechanism by which radiation induces injury and death to normal and tumor tissues remains largely unknown. It is believed that tissue multipotential precursor cells (referred to as "clonogens") are the critical and determinant targets of radiation (1, 2). Clonogens are loosely defined as cells within a tissue or tumor with the capacity to produce a family of descendants and are often referred to as clonogenic "stem" cells (3, 4), without evidence that these are true stem cells capable of producing identical daughter progeny. Although the precise identity of tissue clonogens remains elusive, it is a firmly held belief that clonogen depletion is required for the induction of permanent tissue damage or successful tumor eradication. Although this paradigm has served as the basic tenet for the use of radiation in the treatment of human tumors, it has not been validated in any type of tissue *in vivo*, because systems that allow identification and tracking of tissue clonogens have not been available.

Studies on the loss of regenerative capacity of mammalian cells irradiated *in vitro* by means of the "clonogenic assay" (5) have indicated that delayed (reproductive or necrotic) cell death is the relevant lethal mechanism for tissue clonogens, as opposed to apoptosis (6). Reproductive cell death is believed to result primarily from the induction of DNA double-strand breaks (7), which, when unrepaired or misrepaired, lead to the progressive accumulation of mutations and chromosomal aberrations as damaged cells undergo divisions. These chromosomal aberrations ultimately lead to lethal mutations and death for the dividing cell. Thus, in contrast to apoptosis, which occurs soon after cytotoxic insult and before cell division, several cell divisions are required for cells to die by reproductive cell death.

If indeed radiation-induced tissue death is attributable to clonogen reproductive cell death, then the inherent sensitivity to radiation should depend on the clonogens' ability to regulate progression through cell cycle checkpoints in coordination with the DNA repair process, referred to collectively as the DNA damage response pathway (DDR; see ref. 8). Consistent with this model, mutations in checkpoint regulators such as ataxia telangiactasia mutant or genes involved in DNA double-strand break repair confer radiosensitivity both *in vitro* and *in vivo* in both normal and tumor tissues (9). Because tumors are believed to arise secondarily to mutations in the DDR pathway (10), they are hypothesized to be more sensitive to cytotoxic therapy than normal tissues. Although this is the paradigm around which cytotoxic therapy is delivered, further genetic understanding of radiation-induced reproductive cell death has not been feasible because of the lack of a tissue model.

Here we have addressed these issues by creating a model of reproductive cell death in the vulva of the nematode *Caenorhabditis elegans*. The *C. elegans* vulva is formed from 22 vulval cells that are the descendants of three vulval precursor cells (VPCs), P5.p, P6.p, and P7.p (11). Under the influence of an inductive signal (LIN-3/EGF) from the anchor cell in the somatic gonad, P6.p, the cell closest to the anchor cell, adopts the primary vulval cell fate and divides three times to generate the cells that form the center of the developing vulva. The cells flanking P6.p (P5.p and P7.p) adopt the secondary cell fate and divide three times to generate the cells that form the sides of the developing vulva. The response of VPCs to LIN-3/EGF is mediated by an EGFR/Ras/MAPK pathway that is highly conserved from *C. elegans* to humans. Adoption of the secondary fate also depends upon lateral signals from P6.p that activate a conserved LIN-12/Notch pathway. Although the remaining three VPCs (P3.p, P4.p, and P8.p) normally receive neither signal and adopt the nonvulval tertiary cell fate, they have the capacity to adopt primary or secondary cell fates if the inner VPCs are ablated (11, 12) or if signaling through the EGFR pathway is enhanced by mutation or transgenic overexpression (13, 14). Thus, all six cells have similar developmental potential and are termed the "vulval equivalence group." Because the VPCs serve as multipotential progenitors for specific vulval cell lineages, they mimic the model of tissue clonogens as described in mammalian systems.

To exploit the opportunity to follow the fate of irradiated VPCs through three mitotic cycles without tissue disruption, we selected the *C. elegans* vulva as a tissue model to explore the reproductive survival of irradiated VPC progeny. Our data show that exposure of larval-stage *C. elegans* to whole-body radiation results in a dose-dependent effect on VPCs. After irradiation, VPCs survive and adopt their cell fates correctly, undergoing the normal three rounds of synchronized cell division to produce a WT L4-stage vulval structure. However, in the L4 and early-adult stages, the postmitotic vulval cells die in a stochastic fashion, leading to the generation of radiation-induced abnormal

Conflict of interest statement: No conflicts declared.

Abbreviations: DDR, DNA damage response; VPC, vulval precursor cell; Pvl, Protruding vulva; Vul, Vulvaless; lof, loss of function.

†To whom correspondence should be addressed. E-mail: joanne.weidhaas@yale.edu.

www.pnas.org/cgi/doi/10.1073/pnas.0603791103

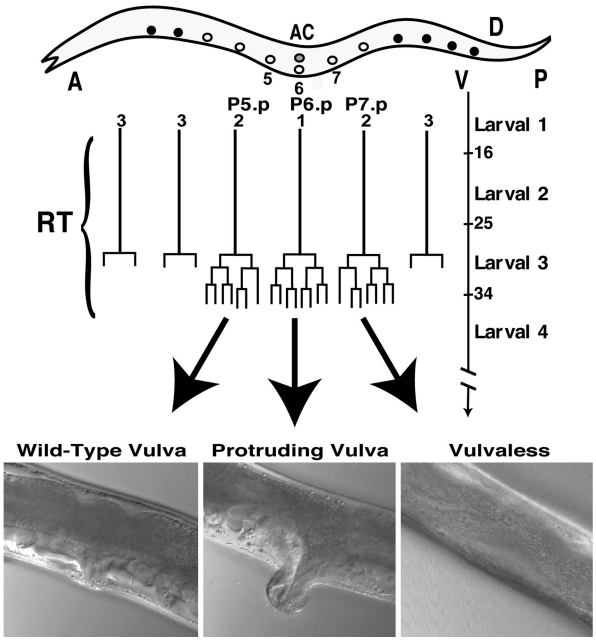

Fig. 1. Radiation causes vulval abnormalities in *C. elegans*. During vulval development, the center three VPCs (P5.p, P6.p, and P7.p) undergo three synchronized divisions. The time of larval stage transitions in hours is listed on the right. Animals treated with radiation (RT) during vulval development exhibit either WT or abnormal vulval phenotypes as adults.

vulval phenotypes. Morphologically and genetically, vulval cells die a nonapoptotic necrotic cell death. This model therefore represents a tissue model of clonogen reproductive cell death and thus acts as a platform to genetically identify the proteins and pathways necessary for tissue clonogen and ultimately normal- and tumor-tissue survival after cytotoxic therapy.

Results

Ionizing Radiation Induces Abnormal Vulval Phenotypes in *C. elegans*. In our hands, exposure of WT *C. elegans* (N2) larvae or adults to radiation with doses of up to 500 Gy did not result in significant animal lethality, similar to reports by others (15). Synchronized animals exposed to radiation from the first to the fourth larval stage do show vulval abnormalities as adults, however, with animals developing a WT vulva or one of the malformed vulval phenotypes, Protruding vulva (Pvl) or Vulvaless (Vul). This time period of radiosensitivity spans the period of the three synchronized vulval cell divisions (Fig. 1). *C. elegans* strains treated in our study show no other obvious structural abnormalities after irradiation, except for abnormal gonad development, sterility, and a mild growth delay that is dose-dependent.

To test whether the radiation-induced vulval phenotype was vulval cell-specific, we exploited the fact that *C. elegans* vulval cells are synchronized and tested for cell-cycle-dependent radiosensitivity, as found in mammalian cells (16). Following vulval cells microscopically through their first cell division, we found the greatest resistance to radiation (largest proportion WT phenotype) when radiation was delivered during the period preceding the first vulval cell division, approximating the S phase. In contrast, we found the greatest sensitivity to radiation (smallest proportion of remaining WT vulval phenotype) at the subsequent mitosis, with a similar radioresistance and radiosensitivity peak during the two subsequent vulval cell divisions (Fig. 2*A*, $n = 3{,}780$). This pattern of cell-cycle-dependent radiosensitivity is identical to that found in mammalian cells. Of note, only one additional radiosensitive peak was noted, perhaps

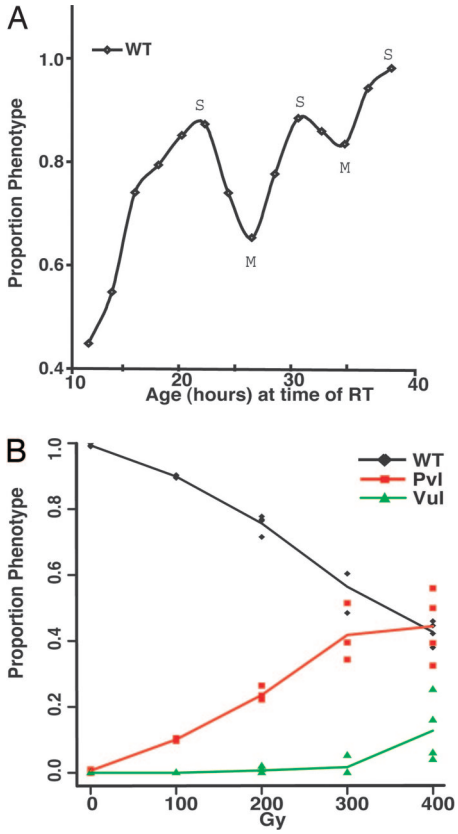

Fig. 2. Abnormal vulval phenotypes are vulval cell-specific and reflect radiosensitivity. (*A*) Radiosensitivity (proportion WT vulva) varies with the vulval cell cycle. Age (hours) corresponds also to the time scale of larval stages in Fig. 1. M, vulval cell mitosis; S, vulval cell S phase. (*B*) The proportion of the three vulval phenotypes varies with increasing dose, with a decrease in the WT phenotype and an increase in the Pvl and Vul phenotypes. Individual sample results are depicted as colored dots for each corresponding dose and phenotype.

because of the very short time between the second and third vulval cell divisions. In addition, resistance to radiation increased between the first and last S phase peak ($P < 0.001$), likely because of fewer vulval cell divisions after irradiation leading to less tissue-damage expression, a finding consistent with reproductive cell death. For consistency and reproducibility, all further experiments were performed at the first S phase radioresistance peak, determined individually for each strain.

Finally, the proportion of animals exhibiting abnormal vulval phenotypes after irradiation increased in a dose-dependent manner with a similar decrease in the WT phenotype (Fig. 2*B*, $n = 2{,}769$). Although the Pvl phenotype has a lower-threshold dose than the Vul phenotype, the abnormal vulval phenotypes have similar slopes, suggesting they may be due to a related process. These findings support the hypothesis that vulval abnormalities after irradiation in *C. elegans* represent radiation-induced vulval cell death.

Abnormal Vulval Phenotypes Are Due to Reproductive Vulval Cell Death. Pvl and Vul phenotypes can be caused by a reduction in the number of vulval cells or by defective vulval morphogenesis, both of which can be caused by defects in VPC fate specification or execution or pre- (apoptotic) or postmitotic (reproductive) VPC or vulval cell death (17). To determine which types of defects lead to Pvl and Vul in our system, vulval cell lineage analysis (enabling tracking of individual vulval cell production) was performed on N2 animals after 400 Gy of irradiation. Although at this dose >50% of the animals exhibit abnormal

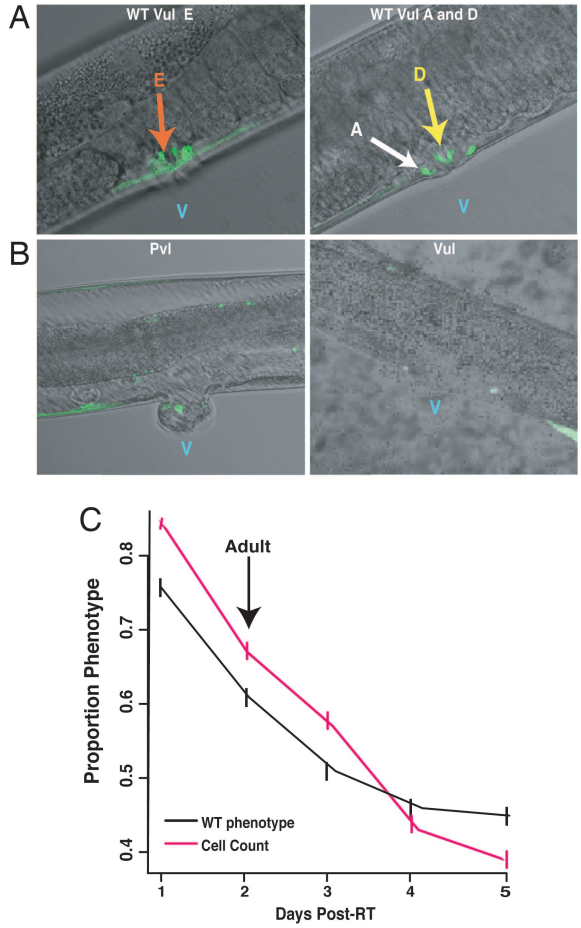

Fig. 3. Abnormal vulval phenotypes are due to vulval cell loss. (*A*) In *syIs49*, a subset of vulval cells (VulE, A and D cells; labeled E, A, and D) express a ZMP::GFP fusion protein, allowing direct visualization. V, vulva. (*B*) In Pvl and Vul animals, the fluorescent vulval cells are lost, with one fluorescent cell seen in the Pvl animal and none in the Vul animal. (*C*) After 400 Gy, the kinetics of fluorescent cell loss parallels the gradual decrease in the WT phenotype, most of which occurs after the animals reach adulthood.

vulval phenotypes as adults, in every case the VPCs complete all of their divisions after irradiation ($n = 30$). These findings indicate that VPCs function appropriately after irradiation, and that vulval abnormalities are not due to VPC or premitotic vulval cell loss.

To next determine whether vulval abnormalities are due to defective vulval morphogenesis, N2 *C. elegans* irradiated with 400 Gy were isolated and examined at the L4 stage. Normally, after completion of the cell divisions, the vulval cells undergo a series of morphogenic movements and cell fusions to form a symmetric vulval invagination in the L4 stage. Using Nomarski optics, normal vulval structures were identified in 98% of L4 *C. elegans* ($n = 100$) after irradiation, although only 43% of the animals in these studies displayed WT vulvae as adults. These findings confirm that the great majority of vulval cell fate decisions and morphogenic movements are normally executed up to the L4 stage of development after irradiation.

We next used a *C. elegans* strain (*syIs49*) expressing a GFP reporter (ZMP-1::GFP; strain contains an integrated transgenic array) expressed in 10 of the 22 vulval cells, beginning in late L4 (VulD and VulE) or young adulthood (VulA) and persisting through the adult stage (ref. 18; see Fig. 3*A*). Use of *syIs49* allows identification and tracking of individual postmitotic vulval cells. Because postmitotic vulval cells normally exist in different focal planes, and abnormal vulval phenotypes further distort the normal vulval anatomy, confocal microscopy was used to both identify and quantify these cells. First, fluorescent vulval cells were identified in individual *syIs49* L4-stage animals irradiated with 400 Gy, and animals were followed through adulthood ($n = 10$). Although all fluorescent vulval cells were present at the L4 stage in each animal studied, these cells gradually disappeared after irradiation in 5 of 10 animals, a finding associated with the development of abnormal vulval phenotypes (Fig. 3*B*). To better evaluate the kinetics of vulval cell loss, fluorescent vulval cell counts and the WT vulval phenotype were scored in animals every 24 h until day 5 after 400 Gy of irradiation. The finding that fluorescent vulval cell loss closely parallels the decrease in the WT phenotype (Fig. 3*C*, $n = 118$) supports the hypothesis that vulval cell loss is responsible for the development of abnormal vulval phenotypes after irradiation.

To confirm that our WT phenotypic readout is an accurate representation of vulval cell death, we next performed dose–response curves and compared the proportion of WT vulval phenotype and the total fluorescent cell count at each dose. There was a clear correlation between the decrease in the WT phenotype and the loss of ZMP-1::GFP-positive vulval cells with increasing dose (Fig. 6, which is published as supporting information on the PNAS web site; $n = 300$). In addition, the number of remaining fluorescent cells correlated with the severity of the vulval phenotype in these studies, with control unirradiated or irradiated WT animals having significantly more fluorescent vulval cells than Pvl animals ($P < 0.01$ vs. WT) or Vul animals ($P < 0.01$ vs. WT and $P < 0.01$ vs. Pvl; Table 1, which is published as supporting information on the PNAS web site).

The above findings support the hypothesis that radiation-induced vulval cell loss causes the vulval abnormalities in our model, and that the remaining proportion of animals displaying the WT phenotype after irradiation is a measure of cellular radiosensitivity. In addition, evidence that irradiated VPCs undergo three normal divisions, execute characteristic morphogenic movement, and form well defined tissue structures before dying fits the criteria of classic reproductive cell death.

Vulva Cell Death Is Nonapoptotic Necrotic Cell Death. In *C. elegans*, both apoptotic cell death as well as necrotic cell death have been morphologically and genetically described (19–23). Apoptotic cell death after genotoxic insult with radiation is morphologically similar to programmed cell death, with classic pyknotic cells (21). Of note, in this study, no apoptosis was identified in somatic tissues (such as the vulva) after radiation. Genetically, radiation-induced apoptotic cell death is abolished in animals in which the apoptotic program is genetically inactivated, including animals harboring mutant alleles for the BCL2 homologue, CED-9 [*ced-9(n1950)*] and Caspase [*ced-3(n717)*; ref. 21].

Necrotic cell death in *C. elegans* is genetically induced in neuronal cells in animals harboring a mutant *mec-4* receptor and is associated with "necrotic vacuoles" (23, 24). Necrotic cell death is genetically distinct from apoptotic cell death, because it is not significantly altered by mutations in CED-9 or the Caspase proteins (23). In contrast, necrotic cell death in *C. elegans* genetically requires the same cell corpse removal pathway as apoptotic cell death, including the engulfment protein CED-1 (25, 26).

To better morphologically characterize vulval cell death in our model, we followed irradiated *C. elegans* subsequent to the L4 stage with Nomarski optics. Pyknotic cells were not identifiable in the vulva, although we were able to identify vacuoles occupying the space where vulval cells should be, likely representing vulval cell corpses (Fig. 4*A*, $n = 93$). The pattern of vacuole formation was stochastic and transient, occurring only after the L4 stage, with vacuoles observable in 26% of the animals compared with 4% of unirradiated controls ($P < 0.001$).

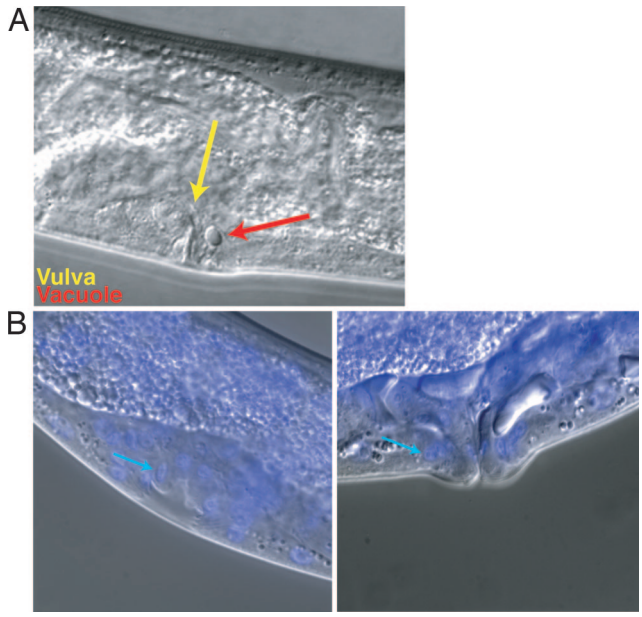

Fig. 4. Vulval cell death is morphologically similar to nonapoptotic necrotic cell death. (*A*) Radiation-induced vulval cell vacuole or corpse. (*B*) Vulval cell (blue arrows) at the L4 stage (*Left*) and the adult stage (*Right*) with Hoescht 33342 staining and Nomarski optics.

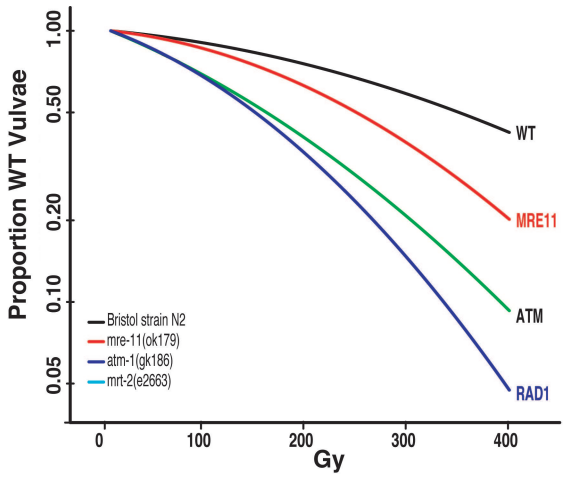

Fig. 5. Dose–response curves of DDR pathway mutants. The WT phenotype after irradiation is plotted against radiation dose for DDR mutant strains compared with N2 (WT) *C. elegans*. Individual sample results are depicted as points. Mammalian protein orthologues are listed at the end of the dose–response curves, and *C. elegans* strain names are in the lower left corner.

To further confirm that the vulval cell death in our model was nonapoptotic, we used apoptotic cell stains previously used in *C. elegans* to document apoptotic cell death after irradiation (20). We easily identified apoptotic cells in the gonad using these stains after radiation, with bright chromatin condensation [DAPI, acridine orange (AO), and Hoescht 33342] or pyknotic cell staining (data not shown, $n = 60$). In contrast, no apoptotic cells were identified in the vulva with these stains. To look more closely at vacuoles, we used morphologic analysis in combination with Hoescht 33342 dye and were able to identify individual vulval cells in the L4 stage through adulthood (Fig. 4*B*, $n = 93$). Vulval vacuoles did not exhibit chromatin condensation but instead had either diffuse or no chromosomal staining (data not shown), consistent with nonapoptotic necrotic cell death. Unfortunately, we were unable to use markers that are specific for necrotic cells such as ethidium bromide or propidium iodide, because these compounds cannot pass through the *C. elegans* gut to reach the vulva cells.

Finally, to determine the genetic basis of the vulval cell death in our system, we tested the vulval radiosensitivity of CED-9 [*ced-9(n1950)*], Caspase [*ced-3(n717)*], and ABL [*abl-1(ok171)*] mutant animals, shown to have altered apoptotic cell death after irradiation (21, 27). There was not a significant difference in vulval radiosensitivity (as evaluated through dose–response curves) compared with N2 animals ($n = 2{,}658$) in these strains (Table 2, which is published as supporting information on the PNAS web site). We next tested an animal with a mutant CED-1 protein [*ced-1(e1735)*], found to be deficient in cell corpse removal in both apoptotic and necrotic cell death (25). Radiosensitivity (as measured by the WT phenotype) was not significantly different between N2 and *ced-1(e1735)* animals ($n = 1{,}427$ for CED1). However, between the L4 stage and adulthood, there was a significantly greater number of cell corpses (vacuoles) in *ced-1(e1735)* animals compared with N2 animals (50% vs. 27%, $P < 0.03$, $n = 126$), supporting the hypothesis that these vacuoles are indeed cell corpses and indicating the requirement of the CED-1 protein for their removal. These findings confirm that the vulval cell death in our system is morphologically and genetically similar to necrotic cell death and unique from apoptosis, thus consistent with radiation-induced reproductive cell death.

The DDR Pathway Protects from Reproductive Vulval Cell Death. The *C. elegans* DDR pathway is highly conserved to the mammalian DDR pathway, as evidenced by functional genomic mapping (28). The existence of cell cycle checkpoint arrest in *C. elegans* after irradiation was previously proven in studies of the germ line (21), where strains with mutations in checkpoint proteins HUS1, MRT2, and CLK-2 are resistant to apoptotic cell death, exhibiting radioresistance. We reasoned that *C. elegans* strains with mutations in the DDR pathway, in contrast, should be sensitive to reproductive cell death and exhibit radiosensitivity. We thus tested the DDR mutant strain *clk-2(mn159)* (29) and found that *clk-2(mn159)* was significantly radiosensitive ($P < 0.003$ vs. N2). To confirm that cell death in *clk-2(mn159)* is reproductive cell death, we scored *clk-2(mn159)* at the L4 stage after irradiation and found that all of the L4 structures were normal after 400 Gy (100%, $n = 100$), as seen in N2 animals.

Thereafter, we conducted a survey of all viable *C. elegans* strains with single-gene loss-of-function (lof) mutations of the DDR pathway, including RAD1/*mrt-2(e2663)*, HUS1/*hus-1(op241)*, MRE11/*mre-11(ok179)*, MSH2/*msh-2(ev679::Tc1)*, MSH6/*msh-6(pk2504)*, ATM/*atm-1(gk186)*, P53/*cep-1(gk138)*, and WEE1/*wee-1.1(ok418)*. These strains are significantly radiosensitive in our system compared with N2 *C. elegans*, with the exception of MSH6 (Fig. 5*A*, Table 2). Because not all of these mutations are null alleles, conclusions regarding differences in the degree of radiosensitivity between these mutants are not possible.

One of the final steps before arrest at the cell cycle checkpoint is the degradation of the CDC25 protein. In *C. elegans*, there are four CDC25 proteins, which have high sequence homology and likely partially redundant functions (30). *C. elegans* strains containing a gain-of-function (gof) CDC25 protein [*cdc25.1(ij48)*, with an accelerated cell cycle checkpoint (31)] as well as a strain with a lof CDC25 protein [*cdc-25.3(ok358)*, with a prolonged checkpoint] both exist. The *cdc25.3(gof)* mutant displayed radiosensitivity when compared with N2 *C. elegans*, whereas the *cdc25.3(lof)* mutant was radioresistant in our system ($P < 0.05$ vs. N2 for each; see Table 2).

As controls, we tested the radiosensitivity of *C. elegans* strains

GENETICS

with mutations in proteins involved in DNA repair by means of the meiotic recombination pathway but not the DDR pathway [SPO-11/*spo-11(ok79)* and MSH-5/*msh-5(me23)*; see ref. 32]. These strains did not display significant radiosensitivity when compared with WT N2 *C. elegans* (Table 2).

To further validate our system, we performed epistasis experiments between two proteins of the DDR pathway: the radioresistant *cdc25.3(lof)* mutant and the radiosensitive *hus-1(op241)* mutant. CDC25 is epistatic to HUS1 (see *Supporting Text*, which is published as supporting information on the PNAS web site), indicating that our model is able to appropriately order proteins in the radioresponse.

Our findings that lof mutants of the DDR pathway manifest markedly enhanced radiation sensitivity in a model of reproductive cell death provide confirmatory evidence at the tissue level that residual DNA damage is the cause of reproductive cell death. As such, this *C. elegans* model represents an *in vivo* tissue model appropriate for identifying and ordering additional genetic pathways necessary for protection from reproductive cell death.

Discussion

We have created a tissue model of radiation-induced reproductive cell death in the vulva of the nematode *C. elegans*, a tissue with multipotential precursor cells resembling human tissue clonogens. Reproductive cell death is considered the primary mechanism of radiation-induced clonogen cell death, resulting in tissue injury and tumor eradication. This work confirms that reproductive death of the VPCs is sufficient to lead to tissue death, as predicted for human clonogens. Because this model of reproductive cell death is in isolation of apoptotic cell death, we were able to contrast the genetic programs used in these unique forms of cell death. Additionally, we have confirmed that the DDR pathway is critical for clonogen cell survival and have proven the utility of our system for epistasis analysis. This work indicates the potential use of this *C. elegans* tissue model of reproductive clonogen cell death ("Radelegans") for further identification and ordering of the proteins and pathways necessary for clonogen survival after irradiation.

The radiation doses used in Radelegans to produce vulval malformations (100–400 Gy) are approximately two logs higher than those typically used to study biologic responses in mammalian cells (0.5–10 Gy). The need for higher dose levels in *C. elegans* is consistent with the observation that the dose required to produce a given biological effect in eukaryotic cells is inversely related to the size of the genome (33, 34). Although the inherent cellular sensitivity (termed the D_0) for *C. elegans* has not been established experimentally, calculation of its expected value based on a genome size of 9.7×10^7 nucleotides (35) yields a value of 67.4 Gy. This value resembles the dose required to produce vulval malformations and indicates that doses used in Radelegans are biologically equivalent to the dose range used to generate similar cellular responses in mammalian cells. Although *C. elegans* have an unusual holocentric chromosomal structure, this does not appear to significantly impact the radioresponse in Radelegans [or in previously described models of apoptotic cell death (21)].

Although we did not follow radiation-induced DNA damage in Radelegans to directly measure radiation damage, we were able to identify an easily discernable phenotype representing radiosensitivity. Although others have identified the vulva as a somatic tissue exhibiting radiosensitivity (32), they did not evaluate abnormal vulval phenotypes separately from other developmental damage. We found we were able to specifically target the vulva by delivering radiation to the animals as a synchronized population at a specific time in development, perhaps because the vulva is one of the few organs dividing postembryonically. Although radiation is delivered only during the vulval cell's first S phase, we expect that our findings are applicable to the radiation response of cycling tissues and tumors, because many resistance mechanisms are also cell-cycle-specific.

In Radelegans, cell death was morphologically and genetically unique from apoptotic cell death and similar to necrotic cell death as described in *C. elegans*, occurring independently of the apoptotic machinery but requiring the cell-corpse engulfment protein CED-1. Necrotic cell death in *C. elegans* requires Ca+ influx (24), as does radiation-induced reproductive/necrotic cell death in mammalian cells. Interestingly, we found that animals with mutations in the checkpoint proteins RAD1, HUS1, CLK-2, and P53 were radiosensitive in Radelegans, a phenotype opposite that reported in the *C. elegans* apoptotic cell death model (21). These findings suggest that the role of the checkpoint in the radioresponse is dictated by the destined outcome for the cell: for cells that are dispensable and destined to undergo apoptosis, the checkpoint is required for cell death (36); for cells that are critical and destined to undergo attempted repair, the checkpoint is necessary for survival. A similar role of the checkpoint has been identified in mammalian development, where p53 mutations are protective in mouse cells destined to undergo apoptosis because of an aborted checkpoint (37).

We will continue to use Radelegans to identify and order the pathways involved in reproductive clonogenic cell death after cytotoxic therapy. Through the use of Radelegans, we hope to develop a better understanding of the mechanisms of tumor resistance as well as to identify novel targets to allow future manipulation of normal and tumor-tissue responses to cytotoxic therapy.

Experimental Procedures

Mutations and Strains. Methods for culturing, handling, and genetic manipulation of *C. elegans* were as described by Brenner (38), unless otherwise indicated. The animals referred to here as WT *C. elegans* correspond to the Bristol strain N2. Strains used in this study were obtained from the *C. elegans* Genetics Center unless otherwise noted (see *Supporting Text*).

Synchronization and Radiation of *C. elegans*. Gravid hermaphrodites were washed off plates and digested with an NaOH and bleach solution. The resulting embryos were washed with 1× PBS, plated on unseeded agarose-containing Petri dishes, and placed at 20°C for 14 h. Larvae were transferred to *Escherichia coli* OP50-seeded plates and were considered 1 h old upon placement on food. For radiation, *C. elegans* were placed in a 15-ml conical tube (Falcon) with OP50-seeded agarose and treated in the high-dose-rate position in a Cs^{137} irradiator (Mark I Model 68). The radiation dose was calibrated with a thermoluminescent dosimeter and thin-window ion chamber under conditions simulated for *C. elegans*. After irradiation, *C. elegans* were immediately transferred to a fresh OP50-seeded plate and grown at 20°C to adulthood without disturbance and with adequate food.

Phenotypic Characterization. To examine radiation-induced vulval malformations, treated animals were anesthetized with 5 mM levamisole HCl, placed onto 2% agarose pads, and examined using ×40 Nomarski optics. Postirradiation assessments are performed on adult *C. elegans* at the point of phenotypic stabilization; animals receiving 100–200 Gy are scored on day 3 after irradiation, and animals receiving 300–400 Gy are scored on day 4. All strains are normalized to their 0-Gy data point to rule out any vulval defects independent of irradiation. Because animals are sterile at the doses of radiation used, we classified worms as Vul when there was no identifiable vulval tissue in contrast to standard "bag of worms" scoring.

Determination of Cell Cycle Peak Radiosensitivity. Synchronized larval stage animals were treated with 100 Gy every 2 h from 11

to 39 h of age, with >100 animals per sample. Experiments were repeated two to four times, and values were averaged. For identification of the first S phase for each strain used in this study, populations of synchronized animals were treated with 100 Gy every 2 h from 16 to 24 h of age and scored for vulval phenotype as adults. The time point showing the greatest radioresistance (greatest proportion of WT vulvae) was considered the peak of the first S phase. This was microscopically confirmed for the first five strains used in these studies.

Dose–Response Curves. Dose–response curves were generated at the first S phase radioresistance peak by dividing synchronized *C. elegans* populations into individual feeding plates and treating each dose point sequentially, with a start and an end same-dose control sample. For each dose studied, a minimum of 100 animals were studied per experiment, and experiments were repeated two to four times.

Documentation of Vulval Cell Death. To perform lineage analysis, *C. elegans* were plated on microscope slides on agarose rings, allowing the tracking of single animals. Worms were followed immediately after irradiation until completion of all vulval cell divisions using Nomarski optics at ×100 magnification. Ten individual animals from three separate radiation experiments were scored by using this technique.

To evaluate L4 stage structures, irradiated *C. elegans* were followed after radiation and isolated at the L4 stage by using Nomarski optics. L4-stage vulval invaginations were scored as normal or abnormal under ×100 magnification. Experiments were repeated twice with 50 animals in each sample.

For fluorescensce studies, the *syIs49[pMH86dpy-2(+) + pJB100 (zmp-1*::*GFP)]IV* strain was irradiated and then underwent phenotypic characterization with Nomarski optics and confocal microscopy. Animals were individually followed every 12 h beginning at the L4 stage until day 5 after radiation. Experiments were expanded and repeated twice with 20–30 animals evaluated at each time point, and values were averaged. For comparison of WT phenotype and fluorescent cell counts, 30 animals were evaluated at each dose, and both phenotype and cell counts were scored. Experiments were repeated twice, and standard deviation was calculated for each data set and averaged.

To determine cell morphology, animals were viewed under ×100 magnification with oil with a Zeiss-Axiotome microscope. DAPI, acridine orange, Syto 12, and Hoescht 33342 staining were done per standard *C. elegans* protocols. Animals were viewed with the appropriate fluorescent filters, and images were taken by using a Zeiss camera attached to the microscope.

To score cell corpses, animals were treated with 400 Gy, stained with Hoescht dye, and followed every 6 h after the L4 stage until they reached adulthood (24 h). Counts were averaged, and a *t* test was used to calculate significance.

Strain Construction and Analysis. Double mutants were generated by using standard genetic methods. The presence of both mutant alleles was confirmed by single-animal PCR. Primers for alleles were designed based on the *C. elegans* Genetics Center recommendations.

Statistical Analysis. The dose–response curves were obtained by using a linear fit to the data (proportion of WT) after Box-Cox transformation. For each of the strains, the logarithm of the proportion of WT worms was modeled as a quadratic function dose of the form $\log(\text{prop WT}) = A \times \text{dose} + B \times \text{dose}^2$. The least-squares fit of the coefficients A and B were used to draw the dose–response curves in the figures. Each of the mutant strains was compared against the WT by using a stratified two-sample Wilcoxon rank sum test. This procedure uses the test statistic obtained by taking the sum of the two sample rank sums for comparing the two strains within each dose level and standardizing them appropriately. Stratified *t* tests are performed to analyze significance for all cases.

Special thanks to Steven Leibel for his support and Lisa Cabral for her editing expertise. This work was supported by Radiological Society of North America Holman seed grant funding (to J.B.W.) and by National Science Foundation Grant IBN-0235922 (to D.M.E.). Nematode strains used in this work were provided by the *C. elegans* Genetics Center, which is funded by the National Institutes of Health National Center for Research Resources.

1. Hewitt, H. B. & Wilson, C. W. (1960) *Br. J. Cancer* **14,** 186–194.
2. Baker, F. & Sanger, L. (1991) *Int. J. Cell Cloning* **9,** 155–165.
3. Stuschke, M., Budach, V., Klaes, W. & Sack, H. (1992) *Int. J. Radiat. Oncol. Biol. Phys.* **23,** 69–80.
4. Tarnawski, R., Kummermehr, J. & Trott, K. R. (1998) *Radiother. Oncol.* **46,** 209–214.
5. Puck, T. T. & Marcus, P. I. (1955) *Proc. Natl. Acad. Sci. USA* **41,** 432–437.
6. Brown, M. & Wilson, G. (2003) *Can. Biol. Ther.* **2,** 477–490.
7. Elkind, M. M. & Whitmore, G. F. (1967) *The Radiobiology of Cultured Mammalian Cells* (Gordon & Breach, New York).
8. Li, L., Story, M. & Legerski, R. J. (2001) *Int. J. Radiat. Oncol. Biol. Phys.* **49,** 1157–1162.
9. Girard, P. M., Foray, N., Stumm, M., Waugh, A., Riballo, E., Maser, R. S., Phillips, W. P., Petrini, J., Arlett, C. F. & Jeggo, P. A. (2000) *Cancer Res.* **60,** 4881–4888.
10. Hartwell, L. H., Szankasi, P., Roberts, C. J., Murray, A. W. & Friend, S. H. (1997) *Science* **7,** 1064–1068.
11. Sternberg, P. W. & Horvitz, H. R. (1986) *Cell* **44,** 761–772.
12. Sulston, J. E. & White, J. G. (1980) *Dev. Biol.* **78,** 577–597.
13. Beitel, G. J., Clark, S. G. & Horvitz, H. R. (1990) *Nature* **348,** 503–509.
14. Han, M. & Sternberg, P. W. (1990) *Cell* **63,** 921–931.
15. Hartman, P., Goldstein, P., Algarra, M., Hubbard, D. & Mabery, J. (1996) *Mutat. Res.* **363,** 201–208.
16. Sinclair, W. K. & Morton, R. A. (1966) *Radiat. Res.* **29,** 450–474.
17. Joshi, P. & Eisenmann, D. M. (2004) *Genetics* **167,** 673–685.
18. Inoue, T., Sherwood, D. R., Aspock, G., Butler, J. A., Gupta, B. P., Kirouac, M., Wang, M., Lee, P.-Y., Kramer, J. M., Hope, I., *et al.* (2002) *Mech. Dev.* **119,** Suppl. 1, S203–S209.
19. Sulston, J. E. & Horvitz, H. R. (1977) *Dev. Biol.* **56,** 110–156.
20. Gumienny, T. L., Lambie, E., Harwieg, E., Horvitz, H. R. & Hengartner, M. O. (1999) *Development (Cambridge, U.K.)* **126,** 1011–1022.
21. Gartner, A., Milstein, S., Ahmed, S., Hodgkin, J. & Hengartner, M. O. (2000) *Mol. Cell* **5,** 435–443.
22. Driscoll, M. (1992) *J. Neurobiol.* **23,** 1327–1351.
23. Driscoll, M. (1996) *Brain Pathol.* **6,** 411–425.
24. Xu, K., Tavernarakis, N. & Driscoll, M. (2001) *Neuron* **31,** 957–971.
25. Chung, S., Gumienny, T. L., Hengartner, M. O. & Driscoll, M. (2000) *Nat. Cell Biol.* **2,** 931–937.
26. Zhou, Z., Hartweig, E. & Horvitz, H. R. (2001) *Cell* **104,** 43–56.
27. Deng, X., Hofmann, E. R., Villanueva, A., Hobert, O., Capodieci, P., Veach, D. R., Yin, X., Campodonico, L., Glekas, A., Cordon-Cardo, C., *et al.* (2004) *Nat. Genet.* **36,** 906–912.
28. Boulton, S. J., Gartner, A., Reboul, J., Vaglio, P., Dyson, N., Hill, D. E. & Vidal, M. (2002) *Science* **295,** 127–131.
29. Ahmed, S., Alpi, A., Hengartner, M. O. & Gartner, A. (2001) *Curr. Biol.* **11,** 1934–1944.
30. Ashcroft, N. R., Kosinski, M. E., Wickramasinghe, D., Donovan, P. J. & Golden, A. (1998) *Gene* **214,** 59–66.
31. Clucas, C., Cabello, J., Bussing, I., Schnabel, R. & Johnstone, I. L. (2002) *EMBO* **21,** 665–674.
32. Rinaldo, C., Bazzicalupo, P., Ederle, S., Hilliard, M. & La Volpe, A. (2002) *Genetics* **160,** 471–479.
33. Kaplan, H. S. & Moses, L. E. (1964) *Science* **145,** 21–25.
34. Sparrow, A. H., Underbrink, A. G. & Sparrow, R. C. (1967) *Radiat. Res.* **32,** 915–945.
35. *C. elegans* Sequencing Consortium (1998) *Science* **282,** 2012–2018.
36. Tao, W. (2005) *Cell Cycle* **4,** 1495–1499.
37. Nicol, C. J., Harrison, M. L., Laposa, R. R., Gimelshtein, I. L. & Wells, P. G. (1995) *Nature* **10,** 181–187.
38. Brenner, S. (1974) *Genetics* **77,** 71–94.